Journal of Materials Chemistry A

Accepted Manuscript

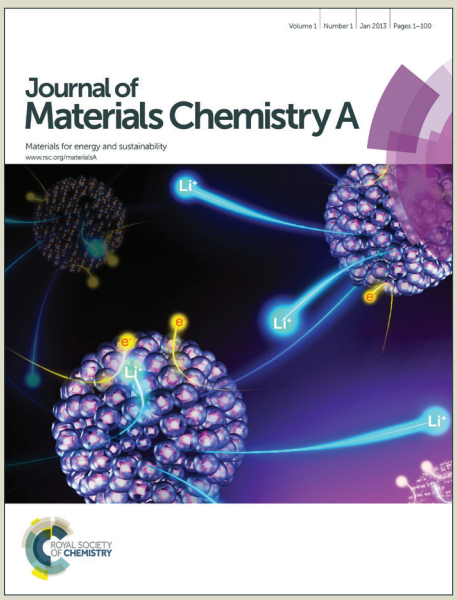

ROYAL SOCIETY OF CHEMISTRY

www.rsc.org/materialsA

Cite this: DOI: 10.1039/c0xx00000x

www.rsc.org/xxxxxx

ARTICLE TYPE

An organosilane-directed growth-induced etching strategy for preparing hollow/yolk-shell mesoporous organosilica nanospheres with perpendicular mesochannels and amphiphilic frameworks

Houbing Zou, [a] Runwei Wang,*[a] Xiaoxin Li, [a] Xue Wang, [a] Shangjing Zeng, [a] Shuang Ding, [a] Lu Li, [a] Zongtao Zhang[a] and Shilun Qiu* [a]

Received (in XXX, XXX) Xth XXXXXXXXX 20XX, Accepted Xth XXXXXXXXX 20XX
DOI: 10.1039/b000000x

We develop an organosilane-directed growth-induced etching strategy to prepare hollow periodic mesoporous organosilica (PMO) nanospheres with perpendicular mesoporous channels and a clear hollow interior as well as an amphiphilic framework. This facile strategy is simple, efficient, and highly controllable. Silica nanospheres were utilized as a hard template to obtain hollow PMOs nanospheres through a one-step route, with the structure parameter highly controlled by adjusting the synthesis conditions. Different organosilanes were used to obtain bridged hollow PMOs nanospheres of different organic groups and showed different directed capacity. The integrity of the bridged organic group was confirmed by Fourier-transform infrared (FT-IR) spectroscopy and solid-state ^{13}C nuclear magnetic resonance (NMR) spectra. Transmission electron microscopy (TEM) observations showed that the growth of the PMO shell and the dissolution of the silica nanosphere core occurred simultaneously for each nanosphere, while ^{29}Si NMR spectra revealed that the dissolved silica species from the silica nanospheres transformed into PMOs shells by co-condensation with hydrolyzed organosilane oligomers. As a result, obtained hollow nanospheres were amphiphilic, which can even be used as a particle emulsifier for O/W or W/O emulsion in various systems. These materials can also be served as an efficient sorbent for removal of hydrophobic contaminants in water. Using the proposed formation mechanism, this strategy can be extended to transform silica-coated composite materials into yolk-shell structures with a functional interior core and a perpendicular mesoporous amphiphilic shell. As a nanoreactor, the -Ph- bridged amphiphilic shell showed faster diffusion rate for organic reactants in water than hydrophilic silica shell, and thus better catalytic activity for reduction of 4-nitrophenol.

Introduction

There has recently been increasing effort focused on the design and fabrication of hollow/yolk-shell nanomaterials due to their fascinating properties of low density, high surface area, permeable shell, and interstitial hollow spaces.[1-10] Hollow/yolk-shell nanostructures have been widely applied in many important research fields[11-31]: nanoreactors,[10-19] drug/gene delivery,[3, 20-25] surface-enhanced Raman scattering technologies,[26] and energy storage and lithium-ion batteries[27-31] because of the unique properties resulting from movable cores, a void space between core and shell, and the wide variability of the core and shell. While several fabrication methods are available: using the Kirkendall[32] or Ostwald ripening effect,[33] ship-in-bottle techniques,[34] bottom-up approaches using soft templating assemblies,[6-8, 35-36] selective etching methods using hard templates[9, 37-39] and self-templating.[10, 40-42] However, the shell material for all of these methods is generally limited to hydrophilic mesoporous silicas. Compared with conventional mesoporous silicas, periodic mesoporous organosilicas (PMOs) are a new class of molecularly organic–inorganic hybrid material with a comparably ordered pore structure and much higher hydrothermal stability.[43-45] Additionally, adjusting the bridged organic groups of PMOs can not only vary pore surface hydrophobicity/hydrophilicity, but also tailor their chemical and physical properties, which can lead to potentially new applications in catalysis, chromatography, sensors, drug delivery, insulating materials and fuel cells.[46-49] Therefore, hollow/yolk-shell PMOs nanoparticles, which combine the unique properties of a hollow/yolk-shell nanoarchitecture with PMOs, is an interesting subject deserving further research. However, to date there have only been a few studies reporting on design of hollow PMOs.[50-58]

There are currently two approaches available for synthesizing hollow PMOs nanoparticles, which can be broadly categorized into soft template methods[50-53, 59] and hard template methods.[55, 57-58] In 2006, Lu and co-workers[50] first synthesized PMOs hollow nanospheres using a vesicle and a liquid crystal dual templating approach. A pluronic F127 block copolymer has also been used as a soft template to synthesize hollow PMOs nanoparticles.[59] Compared with the soft template approach,

using a hard template to prepare hollow/yolk-shell PMOs nanoparticles can better maintain the uniformity and narrow size distribution of the resulting material.[42] Hematite nanoparticles[57] and polystyrene (PS) latex spheres[55] have been used as the hard template to successfully fabricate hollow PMOs nanospheres with uniform particle sizes. Yang's group[56] also reported a structural transformation from a core-shell to a yolk-shell under the assistance of organosilane. Very recently, colloidal hollow PMOs nanospheres were fabricated via a silica-etched chemistry.[58] However, these synthetic procedures involved removal of the core material, resulting in a multistep, complex, and time-consuming process. Furthermore, the mesochannels in the PMOs shell were unordered or worm-like, and did not directly open into the hollow interior, thus limiting their application in catalysis. Moreover, any post-treatment inevitably influenced the mesostructure of the shell material,[9, 37-39] and some ultrasmall fragments remained inside the hollow interior.[60] Therefore, determining a simple, efficient, and controllable strategy to construct hollow/yolk-shell PMOs nanoparticles with an ordered mesostructure and a clear hollow interior remains a significant challenge, and the hydrophilic/hydrophobic property of hollow shell remains unexplored.

Herein, we use the similarity between silsesquioxane chemistry and silica chemistry[61] to develop an organosilane-directed growth-induced etching strategy to prepare hollow PMOs nanospheres with perpendicular mesoporous channels and an amphiphilic framework using monodisperse silica nanospheres as the hard template. To the best of our knowledge, this is the first time a hollow PMOs material with ordered radial mesochannels and an amphiphilic framework has been fabricated through a one-step route. Interestingly, the growth of the PMOs shell and the dissolution of the silica nanosphere core occur simultaneously. The size of the nanospheres and the thickness of the PMOs shell were highly controllable. Different organosilanes were used to obtain different organic group bridged hollow nanospheres, and more hydrophobic the bridged group is, poorer the directed capacity is. These hollow nanospheres exhibited amphiphilicity, which can even be used as a novel kind of particle emulsifier for O/W or W/O emulsion. These materials can also be served as an efficient sorbent for removal of hydrophobic contaminants in water. Furthermore, our strategy can be extended as a general approach to fabricate yolk-shell structures with a functional interior core and a radially oriented mesoporous amphiphilic shell. Prepared Au@Ph-PMOs nanospheres were successfully applied as a nanoreactor for reduction of 4-nitrophenol, and showed higher catalytic activity than hydrophilic Au@SiO_2 nanospheres.

Experimental Section

Chemicals and Reagents

Gold (III) chloride trihydrate ($HAuCl_4 \cdot 3H_2O$, 99.7%), sodium borohydride ($NaBH_4$, 98%), Tetraethylorthosilicate (TEOS, 98%), and aqueous ammonia ($NH_3 \cdot H_2O$, 28%) were purchased from Sinopharm Chemical Reagent Co.Ltd. 1,2-bis(triethoxysilyl)-ethane (BTEE, 96%), 1,4-bis(triethoxysilyl)benzene (BTEB, 96%) and 4,4-bis(triethoxysilyl)biphenyl (BTEBP, 95%) were obtained from Sigma–Aldrich. Cetyltrimethylammonium bromide (CTAB, 99.0 %) was obtained from Huishi Biochemical Reagent Company of China. All chemicals were used as received without any further purification.

Synthesis of monodisperse silica nanospheres

Monodisperse silica nanospheres were synthesized following a modified Stober method. In a typical synthesis, 3 mL of TEOS were rapidly added into a mixture of ethanol (37 mL), deionized water (5 mL), and ammonium aqueous solution (25–28%, 1.6 mL). The mixture was then stirred at room temperature for 2 h, resulting in the formation of a white silica colloidal suspension. The silica particles were collected by centrifugation, washed with deionized water, and stored in 15 mL of ethanol. 0.4 mL of ammonium aqueous solution led to silica nanospheres with 80 nm of particle size.

Synthesis of hollow PMOs (Et-HPMOs) nanospheres

The monodisperse silica nanospheres were utilized as hard template to prepare hollow PMOs nanospheres by a one-step route. In a typical synthesis, 100 mg of the as-prepared SiO_2 nanospheres (or 2 mL of above ethanol solution) were homogeneously dispersed in a mixture containing 22 mL of water and 11 mL of ethanol by ultrasonication for 30 min. After the addition of 0.12 g of CTAB and desired amount of ammonium aqueous solution (25–28%), the resultant mixture was further stirred at room temperature for 30 min. And then, 0.22 mL of organosilane BTEE was solwly dropwise added. After completely hydrolysis of BTEE, the as-obtained white mixture was transferred to a stainless steel autoclave with a Teflon container and hydrothermally treated at 100 °C for 24 h. The hollow PMOs nanospheres were collected by centrifugation and then washed with water and ethanol several times. The surfactant CTAB was removal by refluxing 0.5 g of as-made material in 100 mL of ethanol containing 1.5 g of concentrated HCl aqueous solution for 6 h.

Synthesis of yolk-shell structured Au@Ph-PMOs nanocomposites (YS-Au@Ph-PMOs)

The YS-Au@Ph-PMOs nanocomposites were synthesized under similar reaction conditions for Ph-HPMOs except replacing SiO_2 nanospheres with Au@SiO_2 nanospheres. The detailed synthesis procedure was provided in the Supporting Information.

Absorption of toluene in water

50 μL of toluene was added to 6 mL of water containing 15 mg of Ph-HPMOs nanospheres. The absorption was carried out in a sealed glass vial by equilibrating the mixture for 6 h on a magnetic stirring apparatus. The amount of toluene in water was measured with a UV/Vis spectroscopy.

Catalytic reduction of 4-nitrophenol

Four milligrams of yolk-shell Au@Ph-PMOs nanospheres was homogeneously dispersed in 4.5 mL of deionized water by ultrasonication, followed by the addition of 0.2 mL of 4-nitrophenol solution (1 mM), and the mixture was stirred for 10 min at room temperature. Then, 1.3 mL of $NaBH_4$ aqueous solution (0.2 M), was added to the mixture, which was stirred until the deep yellow solution became colorless. During the reaction, a small portion of the mixture was taken at regular intervals and analysed by UV/Vis spectroscopy.

Characterization

SEM was performed on a Hitachi S-5200 electron microscope. TEM images were obtained on an FEI Tecnai G^2 F20s-twin D573 field emission transmission electron microscope with an accelerating voltage of 200 kV. Powder XRD patterns were obtained by using a Rigaku 2550 diffractometer with Cu Ka radiation (λ=1.5418 °A). N_2 adsorption-desorption isotherms were obtained at -196 ℃ on a Micromeritics ASAP 2010 sorptometer. Samples were degassed at 120 ℃ for a minimum of 12 h prior to analysis. Brunauer–Emmett–Teller (BET) surface areas were calculated from the linear part of the BET plot. Pore size distribution was estimated from the adsorption branch of the isotherm by the BJH method. The total pore volume was estimated from the adsorbed amount at P/P_0 = 0.995. The IR spectra were acquired using a Bruker IFS 66 V/S FTIR spectrometer. ^{29}Si CP-MAS NMR measurements were performed on a Bruker AVANCE III 400 WB spectrometer. The spinning rate was 12 kHz and a total number of 20000 scans were recorded with 6 s recycle delay for each sample. ^{13}C-MAS NMR measurements were performed on Varian Infinity Plus 400 NMR spectrometer. The spinning rate was 4 kHz and a total number of 800 scans were recorded with 4 s recycle delay for each sample. The thermogravimetric analysis (TGA) curve was obtained in a flow of air from 35 to 800 ℃ (10 ℃ min^{-1}) using a Netzsch STA 449C thermogravimetric analyzer. UV-vis spectra were recorded with a Shimadzu UV-2450 spectrometer.

Results and Discussion

Synthesis and characterization of Et-HPMOs nanospheres

Hollow PMOs (HPMOs) nanospheres were prepared using monodisperse silica nanospheres (SNs) as the hard template through a one-step route, owing to the framework similarity between silsesquioxane and silica. Firstly, monodisperse SNs with a mean diameter of 230 nm (Figure 1a) were synthesized through a modified Stober method. And then the SNs solution was diluted through addition of CTAB solution containing NH_4OH (25-28%). After addition and completly hydrolysis of organosilane 1,2-bis(tri-ethoxysilyl)ethane (BTEE) and aging at 100 ℃ for 24 h, uniform -Et- bridged HPMOs (Et-HPMOs) nanospheres with a mean size of 380 nm containing a uniform shell of approximately 75 nm have formed, as shown in Figure 1c to 1e. The hollow space is almost equal to the size of the silica nanospheres, a result of the exemplary hard template action. Note also that the Et-HPMOs nanospheres are well dispersed, and some broken spheres indicated by white arrows also provide evidence of a hollow structure (Figure 1b). In contrast to other hollow mesoporous materials fabricated using a coating-etching route,[40,42,58] the hollow interior is very clear (Figure 1e). From the high-magnification TEM image of the PMOs shell, as shown in Figure 1d, it is clear that the mesochannels are highly ordered and perpendicular to the sphere's surface. Furthermore, a hexagonal pattern, similar to the [110] direction of MCM-41, can be clearly seen in the centre area of the hollow interior, corresponding to the boxed areas in Figures 1e and 1f. Tan found a similar phenomenon in the centre area of mesoporous silica nanospheres with radially oriented nanopores.[62] These results demonstrate that we successfully prepared Et-HPMOs nanospheres with perpendicular mesoporous channels and a clear hollow interior under the direction of organosilane BTEE via a one-step route.

The mesostructure of the PMOs shell was further confirmed by small-angel X-ray diffraction and nitrogen sorption analysis. The small-angel XRD pattern exhibits one sharp diffraction peak and one weak diffraction peak at 2θ values of approximately 2.2 and 4.4 degrees (Figure 2A), indicating an ordered mesopore array. The nitrogen sorption isotherm shows a type IV curve

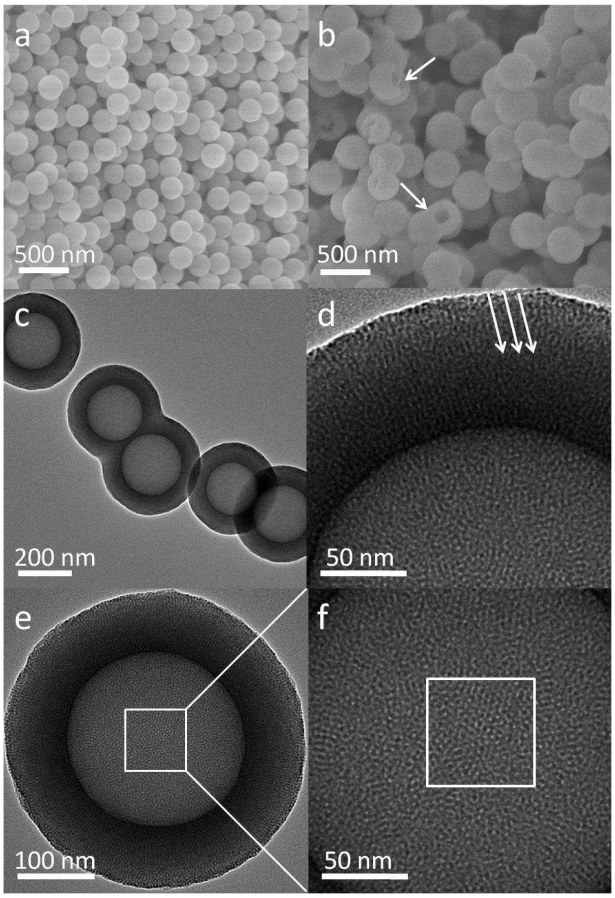

Figure 1. SEM images of (a), monodisperse silica nanospheres, (b), Et-HPMOs nanospheres; (c), low-magnification TEM image of Et-HPMOs nanospheres, (e), TEM image of singel Et-HPMOs nanosphere, (d), (f), high-magnification TEM images of the mesoporous shell and the hollow interior, similar to the [100] and [110] direction of MCM-41, respectively, indicating the hexagonal pattern of PMOs shell.

according to IUPAC classification, with a sharp capillary condensation step in the P/P_0 range of 0.1-0.4 and a distinct hysteresis loop of H3 type in the P/P_0 range of 0.2-0.8. These results show that the Et-HPMOs nanospheres have a mesoporous structure with a uniform pore size. The distinct H3 hysteresis loop indicates that the pores in the PMOs shell directly open into the hollow interior,[56] supporting the idea that a guest molecule could quickly diffuse into the hollow space without obstacle. The corresponding Barrett-Joyner-Halenda (BJH) pore size distribution curve further confirms that the uniform mesopore size centers around 2.0 nm, a size that is smaller than seen for a purely siliceous framework, but frequently found for PMOs materials. The Brumauer-Emmet-Teller (BET) surface area and total pore volume are 520.7 m^2/g and 0.24 cm^3/g, respectively.

The chemical composition of the Et-HPMOs nanospheres was characterized using FT-IR, solid-state ^{13}C NMR and ^{29} Si NMR spectroscopy. Three bands in the range of 2892-2980 cm^{-1}, at 1410 cm^{-1}, and at 1160 cm^{-1} appear in the FT-IR, which we assign to the C-H stretching vibrations, C-H vibration and Si-C vibration, respectively (Figure S1). This result indicates that ethylene groups have been incorporated into the sample. The appearance of resonance at 5.6 ppm in the ^{13}C NMR spectrum (Figure S2), which we assign to the C species of the ethylene

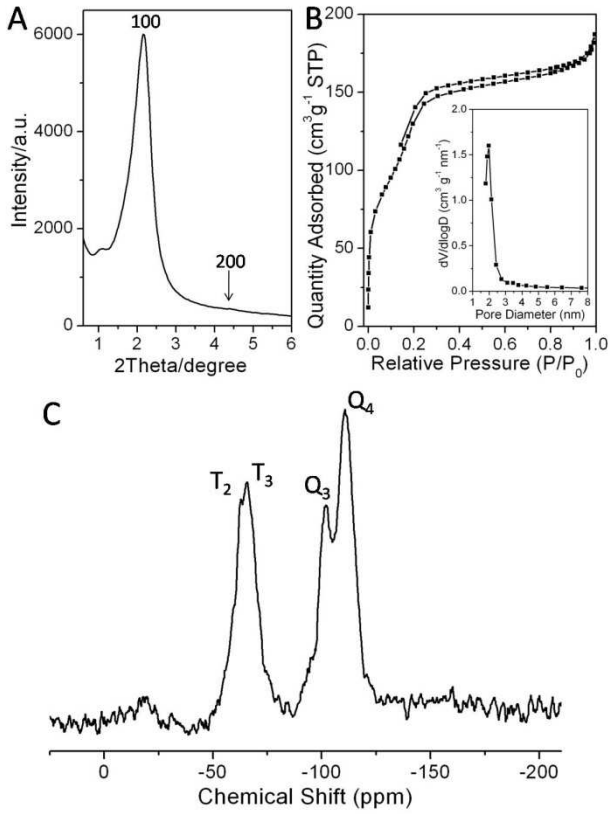

Figure 2. (A) Small-angel XRD pattern, (B) nitrogen sorption isotherm, (C) solid state ^{29}Si NMR spectrum and the inset pore size distribution curve of Et-HPMOs nanospheres.

moiety, further proves the incorporation and integrity of the ethylene organic groups into the PMOs shell. It is notable that the ^{29}Si NMR spectra shows the existence of both T^n and Q^n sites in the range of -50 to -70 ppm and -100 to -115 ppm (Figure 2C), which we attribute to $SiC(OSi)_2(OH)$ (T^2 δ -62) and $SiC(OSi)_3$ (T^3 δ -66) species of silicon attached to ethylene, and the $(HO)Si(OSi)_3$ (Q^3 δ -102) and $Si(OSi)_4$ (Q^4 δ -112) silicon species, respectively.[53,59] The appearance of Q^n sites demonstrates that the dissolved silica species from SNs, considering into no existence of any fragments inside hollow interior, probably co-condensed with hydrolyzed organosilane oligomers and transformed into PMOs shell. Additionally, the high proportion of T^3 and Q^4 reveals the relatively higher degree of condensation, which leads to the much higher hydrothermal stability observed for the HPMOs material.

The thermal behavior of Et-HPMOs nanospheres was investigated by thermogravimetry (Figure S11). In the TG curve for the Et-HPMOs nanospheres, we attribute the weight loss below 100 °C to H_2O molecule being absorbed in the mesochannels of the PMO shell, and attribute the weight loss above 400 °C to the bridged organic group ethylene. There is almost no weight loss in the 100-400 °C temperature range, suggesting that Et-HPMOs nanospheres possess good thermal stability. Furthermore, the weight loss of 7% from 300 to 800 °C is lower than the weight proportion of ethylene in the unit $O_{1.5}Si$-CH_2CH_2-$SiO_{1.5}$ (21%) and indicates the existence of SiO_2 units, a result that is in good agreement with the ^{29}Si NMR spectroscopy results. This phenomenon further proves that the dissolved silica species transform into the PMOs shell.

Engineering the diameter of Et-HPMOs nanospheres and the thickness of Et-PMOs shell

We also demonstrate that this organosilane-directed growth-induced etching strategy is highly controllable. Similar to the fabrication of hollow mesoporous silica nanoparticles through other approaches,[32-42] the structural parameters of the Et-HPMOs nanospheres such as the shell thickness and the particle diameter can be precisely tailored by adjusting the amount of

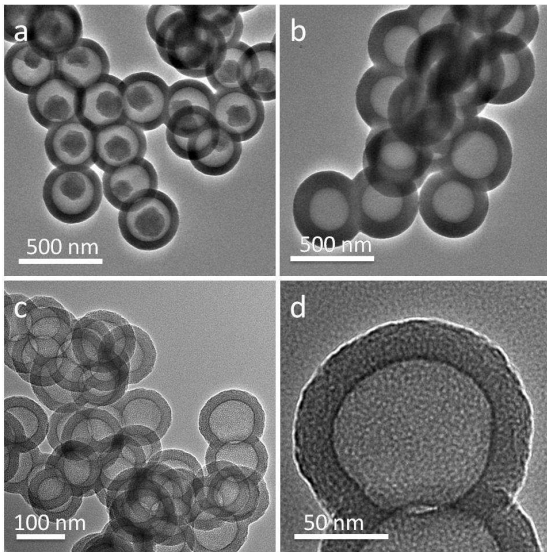

Figure 3. TEM images of Et-HPMOs nanospheres prepared with different amount of organosilane BTEE and different diameter of SNs hard template: a), SiO_2 = 230 nm, BTEE = 0.15 mL; b), SiO_2 = 230 nm, BTEE = 0.27 mL; c, d), SiO_2 = 85 nm, BTEE = 0.22 mL.

organosilane precursor and the size of SNs. As the amount of BTEE increases from 0.15 to 0.27 mL, the shell thickness gradually increases from 50 to 85 nm and the whole particle diameter increased from 330 to 410 nm, respectively (Figure 3a, b). Moreover, the mesochannels in the shell of the PMOs nanospheres are both highly ordered and perpendicular to the spheres' surface (Figure S3, S4). It is worth mentioning that the SNs hard template could not be etched out completely under a low amount of BTEE. Smaller size Et-HPMOs nanospheres were also obtained simply by using SNs of 85 nm as the hard template (Figure 3c, d). However, a lower alkalinity is required when fabricating small diameter Et-HPMOs nanospheres, owing to the relatively lower degree of condensation of the smaller size of SNs. Because of the lower alkalinity, the mesochannels are wormlike, but also directly open into the hollow interior.

Different organic group bridged HPMOs nanospheres

There are hundreds of works published on PMOs materials to date.[46-49] Various bridged organic groups, homogeneously distributed in the pore wall, can lead to different PMOs materials with unique chemical/physical properties.[47] In this work, we tested the ability of other organosilanes such as BTEB and BTEBP to prepare HPMOs nanospheres using the same conditions that were used for Et-HPMOs nanospheres fabrication. Using BTEB, we obtained monodispersed uniform nanospheres approximately 350 nm in diameter (Figure S5), with a uniform

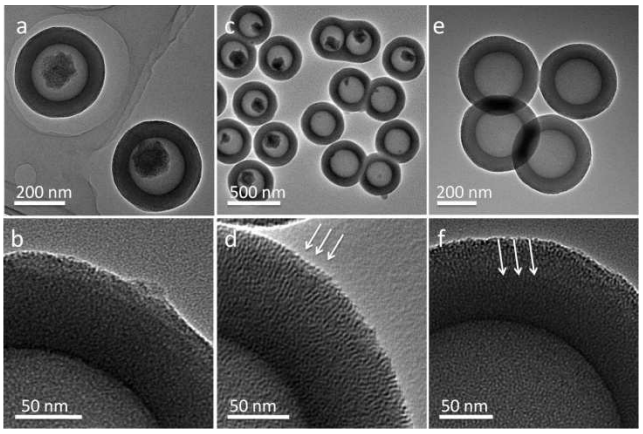

Figure 4. Low and high-magnification TEM images of Ph-HPMOs nanospheres prepared with different amount of ammonium aqueous solution: a, b), 2 mL; c, d), 4 mL; e, f), 6 mL.

Ph-PMOs shell of approximately 65 nm and a void space. However, the hard template of the SNs did not completely dissolve out and the mesochannels are wormlike (Figure 4a, b). As the amount of ammonium aqueous solution increases from 2 to 6 mL, the SNs gradually dissolve out of the final products and the mesochannels transform into highly ordered and perpendicular channels on the surface of the spheres (Figure 4). Meanwhile, the particle diameter of the Ph-HPMOs nanospheres increases from 350 to 390 nm, and the thickness of the shell increases from 65 to 85 nm, respectively. Note also that there is no fragments inside void space in all samples. But it is a pity that -BP- bridged PMOs shell could not form using BTEBP. The nitrogen sorption analysis indicates that the Ph-HPMOs nanospheres possess uniform mesopores centered at 2.1 nm and that directly open into the hollow interior (Figure S6). The BET surface area and total pore volume are calculated to be as high as 1103.2 m^2/g and 0.53 cm^3/g, respectively. The chemical composition of the Ph-HPMOs nanospheres was confirmed by FT-IR, solid-state ^{13}C NMR, and ^{29}Si NMR spectroscopy (Figure S7). These results indicate that different organic group bridged HPMOs nanospheres can be prepared through this growth-induced etching strategy, although different bridged organic groups lead to differences in the directed capacity of the organosilane.

All results above reveal that the growth of PMOs shell and the dissolution of silica nanospheres core occurred simultaneously and the dissolved silica species transform into PMOs shell by co-condensation with hydrolyzed organosilane oligomers. The directed capacity of organosilanes is BTEE > BTEB > BTEBP, which possibly results from the steric effect and hydrophobicity of bridged organic group. More hydrophobic the bridged organic group is, harder the hydrolyzed organosilane oligomers combine with the hydrophilic dissolved silica species. Addtionally, the greater steric effect leads to the slower hydrolysis rate of organosilane. Therefore, the dissolution rate of SNs template is faster when using BTEE as the precursor, and -BP- bridged PMOs shell cannot been formed because of the superior slow hydrolysis rate of BTEBP. Fortunately, adjusting the alkalinity of synthesis system can improve this capacity. Moreover, the alkalinity is responsible for the order degree and the orientation of mesochannels in the PMOs shell. To summarize, the dissolution of SNs template accompanies the growth of PMOs shell, which is determined by the kind and amount of organosilane used to direct the process as well as the alkalinity of the synthesis system.

Formation mechanism of HPMOs nanospheres

To investigate the formation mechanism, TEM was used to monitor the synthesis process of the Et-HPMOs nanospheres, as shown in Figure 5. After complete hydrolysis of the organosilane at room temperature, uniform PMOs shells with a thickness of approximately 55 nm form. Moreover, the size of the SNs hard templates decrease from 230 nm to 130-150 nm as the central void simultaneously, which results from the gradual etching of

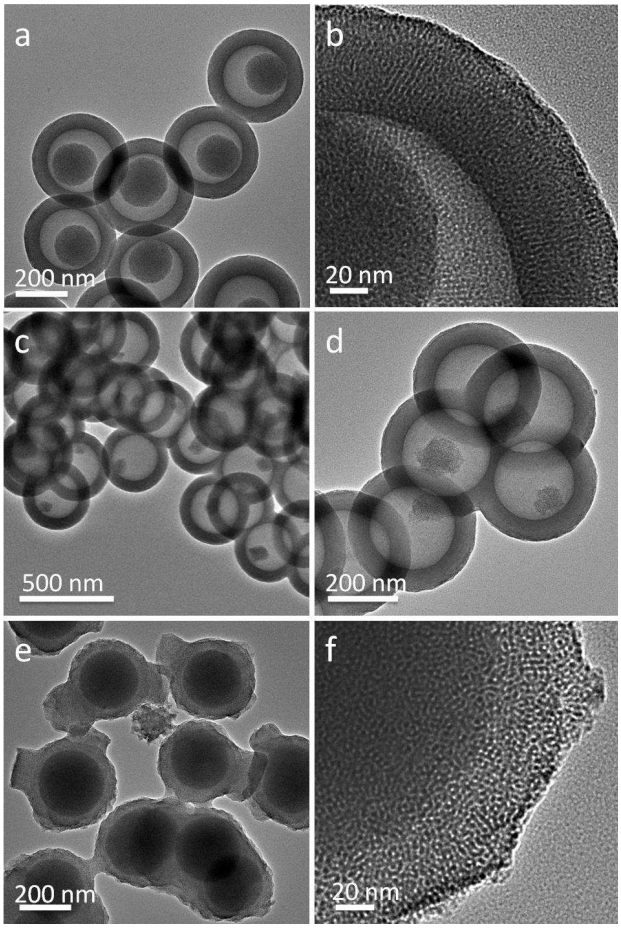

Figure 5. Low and high-magnification TEM images of the samples under various reaction times at 100℃: (a), (b), 0 h, (c), 4 h, (d), 14 h; (e), (f), TEM images of the sample prepared by using inorganic precursor TEOS under the same condition for Et-HPMOs nanospheres.

the SNs templates in the synthesis system (Figure 5a, b). Interestingly, the high-magnification TEM image shows that the

mesopores in the PMOs shells are still ordered and perpendicular to the surface and the void space is very clear, even with a low reaction temperature and short reaction time. When reacting at 100 °C for 4 h, the size of the SNs template further decreases and the thickness of the PMOs shells increases to approximately 60 nm (Figure 5c, d). For each nanosphere, the SNs template was gradually etched and the PMOs shell gradually grows as the reaction progress. After reacting for 24 h, the SNs templates completely etch out and each shell thickness increases to approximately 75 nm, while the hollow space becomes almost equal in size to the SNs template. However, when the organosilane precursor is replaced by the inorganic precursor TEOS, we only obtain core-shell structured SiO_2@mesoporous silica nanospheres with no void space (Figure 5e, f), with some separated mesoporous silica nanoparticles loaded on the surface due to the high alkalinity of the synthesis system. The SNs templates maintain an exact particle diameter while forming an approximately 45 nm mesoporous silica shell. From the high-magnification TEM images (Figure 5f, S8), we can see that the resulting mesochannels in each shell are wormlike but ordered in the separated nanoparticles.

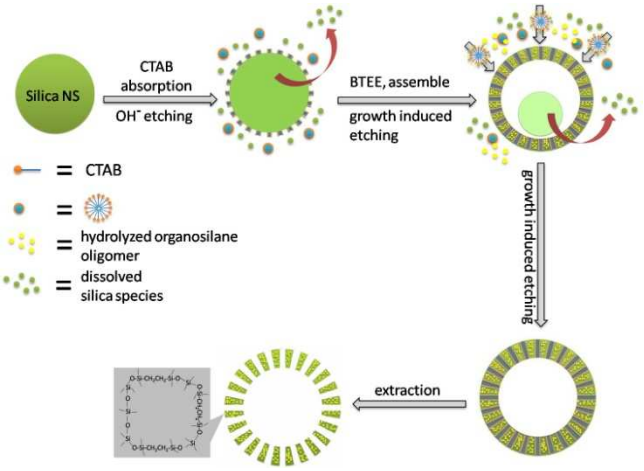

Scheme 1. Schematic illustration for the formation mechanism of the HPMOs nanospheres.

The above results indicate that the formation of such hollow PMOs nanospheres proceeds from the growth of the PMOs shells and the dissolution of the SNs hard templates. The possible formation process of the hollow PMOs nanospheres is illustrated in Scheme 1. First, cetyltrimethylammonium cations (CTA^+) adsorb onto the surface of silica nanospheres through electrostatic interaction, and the SNs etch slightly to allow the system to reach an equilibrium between hydrolysis and condensation.[40] After the addition of organosilane, the results of our ^{29}Si NMR measurements indicate that both the hydrolyzed organosilane oligomers and the dissolved silica species co-assemble with CTAB and co-condense to form PMOs@CTAB composites. Because of the much higher hydrothermal stability of PMOs, the PMOs@CTAB composites fast deposit on the surface of the silica nanospheres, which results in the fast growth of the PMOs shells. Meanwhile, the hydrolysis and condensation balance of the silica species is thoroughly broken and moves towards hydrolysis.[56] In other words, the growth of the PMOs shells promotes the dissolution of the SNs. The SNs continuously dissolve, and the dissolved silica species transform into the PMOs shells through co-condensation with hydrolyzed organosilane oligomers. Finally, the SNs templates completely dissolve out, leading to the formation of Et-HPMOs nanospheres. If we replace the organosilane with the inorganic precursor TEOS while maintaining the same reaction conditions, the hydrolysis and condensation balance of silica species is also broken but moves towards condensation, thus the dissolution of SNs is restrained. In this case, core-shell structured SiO_2@mesoporous silica nanospheres with no void space form rather than hollow mesoporous silica nanospheres.

Compared to Yang's work[56], the critical step is the usage of weak alkaline reagent $NH_3 \cdot H_2O$ and high alkalinity in current system. Both the hydrolysis rate and the condensation rate of silica species get slow in the weak alkaline reagent system. And the dissolution of SNs is gradual from outside to inside. Therefore, the ultrasmall fragments will be also dissolved out, which accompanies with continuous growth of PMOs shell, and then the hollow interior or void space becomes very clear. Moreover, the high alkalinity (pH > 10) is indispensable to the order and perpendicular mesochannels in PMOs shell. If strong alkaline reagent such as NaOH is used, yolk-shell SiO_2@PMOs will be obtained and some ultrasmall fragments exsit inside the void space (Figure S9b, d) under low alkalinity, but uniform PMOs shell could not be formed under high alkalinity. These are the results of fairly fast hydrolysis rate and the condensation rate of silica species. Additionally, it is understandable that the pores in PMOs shell will be unordered or worm-like if the pH value of system is below 10 (Figure 3d, 4a, S9e, f).

Amphiphilicity of HPMOs nanospheres and the application in removal of contaminants in water

The framework of the HPMOs nanospheres is expected to be amphiphilic due to the existence of bridged organic group and SiO_2 units. The Et-HPMOs or Ph-HPMOs nanospheres can both

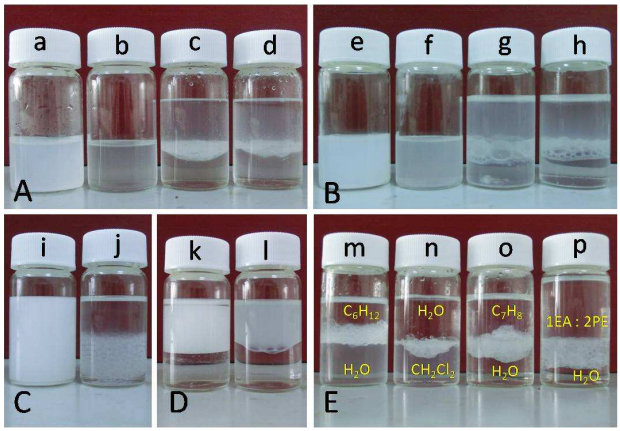

Figure 6. Digital photographs of (A), (a) Et-HPMOs dispersed in H_2O, (b) Et-HPMOs dispersed in CH_2Cl_2, (c) CH_2Cl_2 extracting Et-HPMOs in H_2O, (d) H_2O extracting Et-HPMOs in CH_2Cl_2; (B), (e) Ph-HPMOs dispersed in H_2O, (f) Ph-HPMOs dispersed in CH_2Cl_2, (g) CH_2Cl_2 extracting Ph-HPMOs in H_2O, (h) H_2O extracting Ph-HPMOs in CH_2Cl_2; (C), (i) ethyl acetate extracting Et-HPMOs in water for formation of W/O emulsion, (j) ethyl acetate extracting Ph-HPMOs in water for formation of O/W emulsion; (D), (k) the W/O emulsion of Et-HPMOs being stable enough after standing for ten minutes, (l) the O/W emulsion of Ph-HPMOs disappeared after standing for ten minutes; (E), the O/W or W/O emulsions in various systems of (m) cyclohexane – water, (n) dichloro-methane – water, (o) toluene – water, and (p) 1EA: 2PE - water.

disperse well in water and hydrophobic organic solvent such as cyclohexane, toluene, dichloromethane, chloroform and ethyl acetate. Interestingly, when using water to extract Et-HPMOs or Ph-HPMOs materials dispersed in dichloromethane, we found that some W/O emulsion formed and aggregated in the oil-water interface, with a little of these materials dispersed in water (Figure 6b, d, f, h). Similar phenomena could be observed using dichloromethane to extract these materials dispersed in water (Figure 6a, c, e, g). Additionally, the solubility in ethyl acetate is so well that these materials in ethyl acetate cannot be extracted by water. Using ethyl acetate to extract these materials in water, well W/O emulsion for Et-HPMOs and O/W emulsion for Ph-HPMOs formed at the first. And then the W/O emulsion was stable enough, but the O/W emulsion disappeared and the released Ph-HPMOs materials dissolved in ethyl acetate lay after left undisturbed for ten minutes (Figure 6C, D), suggesting the higher hydrophobility of Ph-HPMOs. Furthermore, well W/O or O/W emulsion in other systems such as cyclohexane - water, toluene - water and 1 ethyl acetate: 2 petroleum ether - water could also be designed through adjusting their composition precisely (Figure 6E). These emulsions keep stable for no less than one month. Based on these results, these amphiphilic hollow nanomaterials can be served as good particle emulsifiers and will be potential in the field of Pickering emulsion.[63]

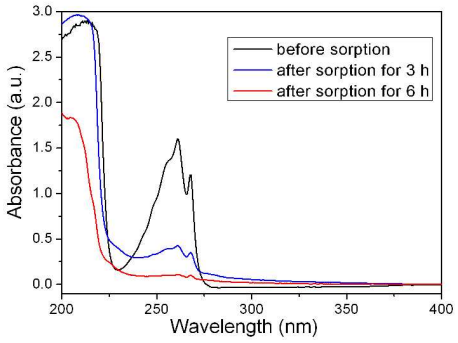

Figure 7. UV spectra of toluene aqueous solution before and after sorption by Ph-HPMOs nanospheres.

We also examined the performance of these amphiphilic hollow nanomaterials in removal of hydrophobic contaminants in water. A saturated toluene solution in water was selected as a model system, and the result is shown in figure 7. It only cost 3 hours to absorb 75% of toluene from its aqueous solution, and most of toluene has been removed after absorbing 6 hours. The sorption capacity has reached to 3 mL/g. These phenomena indicate that the Ph-HPMOs nanospheres possess high sorption efficiency of a superior sorption capacity and a short sorption time, owing to the amphiphilic framework and high BET surface area as well as hollow nanostructure.

Synthesis and catalytic activity of yolk-shell Au@PMOs nanospheres with ordered radial mesochannels and amphiphilic framework

Metal or metal oxide nanoparticles (NP) encapsulated in hollow structures so-called yolk/shell or rattle-type nanostructures have been widely designed and applied in many important research fields, particularly in biomedicine and catalysis.[3,4,11-19] For-example, nanoreactor have been constructed to prevent Au nanoparticles from aggregation for enhancing catalytic activity. However, the shell materials of nanoreactor were limited to the hydrophilic silica or hydrophobic polymer/carbon.[10-19] According to the formation mechanism described above, yolk-shell structured nanoparticles with a functional core and a radially oriented mesoporous amphiphilic shell can be easily prepared by replacing the SNs with silica-coated composites. Using core-shell structured $Au@SiO_2$ nanospheres as templates, shown in Figure 8, we successfully obtained well-defined yolk-shell structures with a

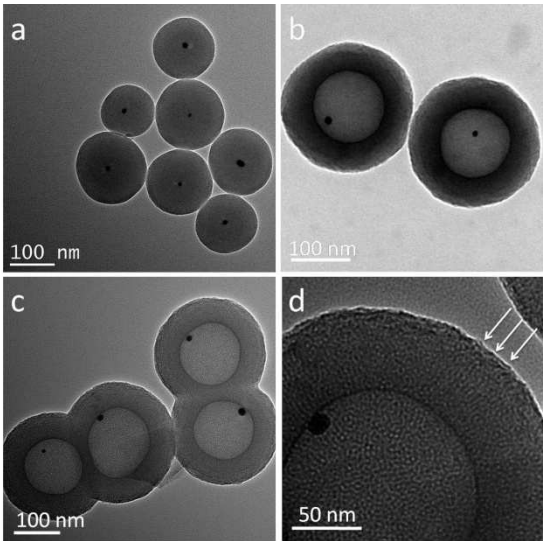

Figure 8. TEM images of (a), $Au@SiO_2$ core-shell nanocomposite, (b), yolk-shell structured Au@Ph-PMOs nanospheres, (c), yolk-shell structured Au@Et-PMOs nanospheres; (d), the corresponding high-magnification TEM image.

movable Au yolk nicely encapsulated within a PMOs shell (designated as YS-Au@PMOs). The organosilane BTEE and BTEB were both approved (Figure 8b, c). The high-magnification TEM image and small-angel XRD pattern (Figure 8d and Figure S11A, respectively) reveal that the mesochannels in the PMOs shells are also highly ordered and perpendicular to the surface, similar to the HPMOs nanospheres prepared from SNs. The wide-angel XRD pattern also verifies the existence of Au nanoparticles (Figure S11B). The -Ph- bridged YS-Au@PMOs nanocomposites show amphiphilicity, too.

The mass transfer directly influences the catalytic performances in heterogeneous catalysis process. The reactant must diffuse into the support and reach the active site where catalytic reaction occurs. We have demonstrated the radially oriented mesoporous amphiphilic shell can enrich hydrophobic organics in water efficiently. Here, the reduction of 4-nitrophenol was selected as a model reaction for testing the catalytic performance of our prepared YS-Au@Ph-PMOs nanocomposites. For comparision, the hydrophilic yolk-shell $Au@SiO_2$ nanocomposites were obtained after calcination of as-made YS-Au@Ph-PMOs nanospheres at 550 ℃ for 6 hours (Figure S12). The reaction mixture went from a deep yellow to colorless gradually. UV-vis absorption spectroscopy was used to monitor the reduction kinetics after the addition of the $NaBH_4$ solution. According to the time-domain spectra, as shown in Figure S13, the absorption of 4-nitrophenol at 400 nm decreases with reaction

time, and a new peak appears at 300 nm as a result of the production of 4-aminophenol.[16,17] The ratio of C_t and C_0, where C_t is the concentration at time t and C_0 is the initial concentration, was measured from the relative intensity ratio of the respective absorbance A_t/A_0 at 400 nm. Figure 9A clearly shows a linear relationship between ln (C_t/C_0) and reaction time for both of the catalysts, indicating that the reaction follows pseudo first-order kinetics. The apparent rate constant K_{app} of the catalyst YS-Au@Ph-PMOs is 5×10^{-3} s^{-1}, calculated directly from the slope of the straight line in Figure 9A. However, the K_{app} of YS-Au@SiO_2

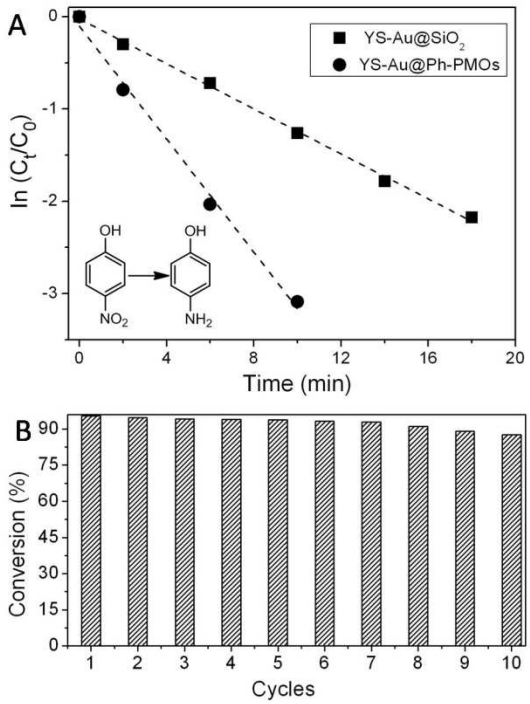

Figure 9. (A), Kinetic analysis of the catalytic reductions. Plot of ln(C_t/C_0) versus time for 4-nitrophenol. (B), Conversions of 4-nitrophenol in 10 successive cycles of reduction with YS-Au@Ph-PMOs.

is only 2×10^{-3} s^{-1}, much lower than that of YS-Au@Ph-PMOs. Moreover, the structural stability of the YS-Au@Ph-PMOs nanocomposites was also examined. After 10 successive cycles, the YS-Au@Ph-PMOs nanocomposites were still stable and active, with a conversion of 88% (Figure 9B). These experimental results indicate that amphiphilic shells support higher diffusion rate for organic reactants in water than hydrophilic shells, and thus better catalytic activity. Therefore, we believe that other metal or bimetal nanoparticles encapsulated in an ordered radial mesoporous amphiphilic shell could be designed for enhancing catalytic activity through this strategy.

Conclusions

In summary, we have reported a novel organosilane-directed growth-induced etching strategy for preparing hollow PMOs nanospheres with perpendicular mesoporous channels and an amphiphilic framework through a one-step route. The growth of each PMO shell and the etching of its silica nanosphere core occur simultaneously, and the growth of the PMO shell promotes the dissolution of the silica nanosphere template. The diameter of the hollow nanospheres and their shell thickness are highly tailored by adjusting the amount of organosilane and the size of the silica nanosphere templates. The mesochannels of the hollow nanospheres are highly oriented, open, and accessible. Different organic group bridged hollow PMOs nanospheres can be prepared through this strategy, and exhibited different hydrophobicity/hydrophilicity. Additionally, more hydrophobic the bridged group is, poorer the directed capacity of organosilane is. These amphiphilic hollow nanomaterials can disperse well in both water and hydrophobic organic solvent, and can be even used as a novel kind of particle emulsifier for O/W or W/O emulsion in various systems such as cyclohexane - water, toluene - water and 1 ethyl acetate: 2 petroleum ether - water. Moreover, as a sorbent for removal of hydrophobic contaminants in water, the -Ph- bridged hollow nanospheres showed ultrahigh sorption efficiency of a superior sorption capacity (i.e., at least 3 $mL\cdot g^{-1}$ of toluene in water) and a short sorption time. Furthermore, this strategy can be extended as a general strategy to prepare yolk-shell structures with a functional interior core and a perpendicular mesoporous amphiphilic shell. Obtained yolk-shell Au@Ph-PMOs nanomaterials were successfully applied as a functional nanoreactor to the catalytic reduction of 4-nitrophenol, and showed higher catalytic activity and stability than hydrophilic Au@SiO_2. Owing to the hollow nanostructures, amphiphilic framework and highly ordered radial mesochannels, the hollow/yolk-shell PMOs nanomaterials reported in this work exhibited excellent performance in the field of sorption of contaminants in water and catalytic reactions proceeding in green solvent water. Moreover, because of the abundant availability of bis-organosilanes, we believe this efficient strategy would offers a platform for designing multifunctional hollow shell nanomaterials for other applications such as drug delivery, bio-imaging, sensing and heterogeneous catalysis.

Acknowledgements

This work was supported by National Natural Science Foundation of China (21390394), the National Basic Research Program of China (2012CB821700, 2011CB808703), NSFC (21261130584, 91022030), "111" project (B07016), Award Project of KAUST (CRG-1-2012-LAI-009) and Ministry of Education, Science and Technology Development Center Project (20120061130012).

Notes and references

[a] *State Key Laboratory of Inorganic Synthesis and Preparative Chemistry, College of Chemistry, Jilin University, 2699 Qianjin Street, Changchun, 130012, China. E-mail: rwwang@jlu.edu.cn, sqiu@jlu.edu.cn.*

† Electronic Supplementary Information (ESI) available: [details of any supplementary information available should be included here]. See DOI: 10.1039/b000000x/

1 F. Caruso, R. A. Caruso, H. Mohwald, *Science* 1998, **282**, 1111.
2 X. W. Lou, L. A. Archer, Z. Yang, *Adv. Mater.* 2008, **20**, 3987.
3 K. An and T. Hyeon, *Nano Today* 2009, **4**, 359.
4 J. Liu, S. Z. Qiao, J. S. Chen, X. W. Lou, X. R. Xing and G. Q. Lu, *Chem. Commun*. 2011, **47**, 12578.
5 Y. Zhao, L. Jiang, *Adv. Mater.* 2009, **21**, 3621.
6 X.-J. Wu, D. S. Xu, *Adv. Mater.* 2010, **22**, 1516.
7 X.-J. Wu, D. S. Xu, *J. Am. Chem. Soc.* 2009, **131**, 2774.
8 J. Liu, S. Z. Qiao, S. B. Hartono, G. Q. M. Lu, *Angew. Chem. Int. Ed.* 2010, **49**, 4981.
9 Y. Chen, H. R. Chen, L. M. Guo, Q. J. He, F. Chen, J. Zhou, J. W. Feng, J. L. Shi, *ACS Nano* 2010, **4**, 529.

10 X. L. Fang, Z. H. Liu, M. F. Hsieh, M. Chen, P. X. Liu, C. Chen, N. F. Zheng, *ACS Nano* 2012, **6**, 4434.
11 J. Lee, J. C. Park, H. Song, *Adv. Mater.* 2008, **20**, 1523.
12 X. Q. Huang, C. Y. Guo, J. Q. Zou, N. F. Zheng, G. D. Stucky, *Small* 2009, **5**, 361.
13 L. F. Tan, D. Chen, H. Y. Liu, F. Q. Tang, *Adv. Mater.* 2010, **22**, 4885.
14 P. M. Arnal, M. Comotti, F. Schüth, *Angew. Chem. Int. Ed.* 2006, **45**, 8224.
15 K. Kamata, Y. Lu, Y. N. Xia, *J. Am. Chem. Soc.* 2003, **125**, 2384.
16 S. Wu, J. Dzubiella, J. Kaiser, M. Drechsler, X. Guo, M. Ballauff, Y. Lu, *Angew. Chem. Int. Ed.* 2012, **51**, 2229.
17 B. Y. Guan, X. Wang, Y. Xiao, Y. L. Liu, Q. S. Huo, *Nanoscale* 2013, **5**, 2469.
18 J. Gaitzsch, D. Appelhans, L. Wang, G. Battaglia, B. Voit, *Angew. Chem. Int. Ed.* 2012, **51**, 4448.
19 X. L. Wu, L. F. Tan, D. Chen, X. L. He, H. Y. Liu, X. W. Meng, F.Q. Tang, *Chem. Eur. J.* 2012, **18**, 15669.
20 S. H. Tang, X. Q. Huang, X. L. Chen, N. F. Zheng, *Adv. Funct. Mater.* 2010, **20**, 2442.
21 Y. Chen , H. R. Chen , S. J. Zhang, F. Chen, L. X. Zhang, J. M. Zhang, M. Zhu, H. X. Wu, L. M. Guo, J. W. Feng, J. L. Shi, *Adv. Funct. Mater.* 2011, **21**, 270.
22 W. R. Zhao, H. R. Chen, Y. S. Li, L. Li, M. D. Lang, J. L. Shi, *Adv. Funct. Mater.* 2008, **18**, 2780.
23 X. Mei, S. Yang, D. Y. Chen, N. J. Li, H. Li, Q. F. Xu, J. F. Ge, J. M. Lu, *Chem. Commun.* 2012, **48**, 10010.
24 Y. F. Jiao, J. Guo, S. Shen, B. S. Chang, Y. H. Zhang, X. G. Jiang, W. L. Yang, *J. Mater. Chem.* 2012, **22**, 17636.
25 L. Y. Zhang, T. T. Wang, L. Li, C. G. Wang, Z. M. Su, J. Li, *Chem. Commun.* 2012, **48**, 8706.
26 M. Roca, A. J. Haes, *J. Am. Chem. Soc.* 2008, **130**, 14273.
27 X. W. Lou, D. Deng, J. Y. Lee, L. A. Archer, *Chem. Mater.* 2008, **20**, 6562.
28 X. W. Lou, C. M. Li, L. A. Archer, *Adv. Mater.* 2009, **21**, 2536.
29 G. Q. Zhang, L. Yu, H. B. Wu, H. E. Hoster, X. W. Lou, *Adv. Mater.* 2012, **24**, 4609.
30 Z. Y. Wang, L. Zhou, X. W. Lou, *Adv. Mater.* 2012, **24**, 1903.
31 A. Q. Pan, T. Zhu, H. B. Wu, X. W. Lou, *Chem. Eur. J.* 2013, **19**, 494.
32 Y. D.Yin, R. M. Rioux, C. K. Erdonmez, S. Hughes, G. A. Somorjai, A. P. Alivisatos, *Science* 2004, **304**, 711.
33 J. Li, H. C. Zeng, *J. Am. Chem. Soc.* 2007, **129**, 15839.
34 M. D. Xiao, C. M. Zhao, H. J. Chen, B. C. Yang, J. F. Wang, *Adv. Funct. Mater.* 2012, **22**, 4526.
35 J. Liu, S. B. Hartono, Y. G. Jin, Z. Li, G. Q. Lu, S. Z. Qiao, *J. Mater. Chem.* 2010, **20**, 4595.
36 Z. G. Feng, Y. S. Li, D. C. Niu, L. Li, W. R. Zhao, H. R. Chen, L. Li, J. H. Gao, M. L. Ruan, J. L. Shi, *Chem. Commun.* 2008, 2629.
37 W. R. Zhao, M. D. Lang, Y. S. Li, L. Li, J. L. Shi, *J. Mater. Chem.* 2009, **19**, 2778.
38 G. G. Qi, Y. B. Wang, L. Estevez, A. K. Switzer, X. N. Duan, X. F. Yang, E. P. Giannelis, *Chem. Mater.* 2010, **22**, 2693.
39 Y. Yamada, M. Mizutani, T. Nakamura, K. Yano, *Chem. Mater.* 2010, **22**, 1695.
40 X. L. Fang, C. Chen, Z. H. Liu, P. X. Liu and N. F. Zheng, *Nanoscale*, 2011, **3**, 1632.
41 X. L. Fang, X. J. Zhao, W. J. Fang, C. Chen, N. F. Zheng, *Nanoscale*, 2013, **5**, 2205.
42 Z. G. Teng, X. D. Su, Y. Y. Zheng, J. Sun, G. T. Chen, C. C. Tian, J. D. Wang, H. Li, Y. Zhao, G. M. Lu, *Chem. Mater.* 2013, **25**, 98.
43 S. Inagaki, S. Guan, Y. Fukushima, T. Ohsuna, O. Terasaki, *J. Am. Chem. Soc.* 1999, **121**, 9611.
44 B. J. Melde, B. T. Holland, C. F. Blanford, A. Stein, *Chem. Mater.* 1999, **11**, 3302.
45 T. Asefa, M. J. MacLachlan, N. Coombs, G. A. Ozin, *Nature* 1999, **402**, 867.
46 F. Hoffmann, M. Cornelius, J. Morell, M. Froba, *Angew. Chem. Int. Ed.* 2006, **45**, 3216.
47 N. Mizoshita, T. Tani, S. Inagaki, *Chem. Soc. Rev.* 2011, 40, 789.
48 W. D. Wang , J. E. Lofgreen , G. A. Ozin , *Small* 2010 , **6** , 2634 .
49 P. Van Der Voort, D. Esquivel, E. De Canck, F. Goethals, I. Van Driessche, F. J. Romero-Salguero, *Chem. Soc. Rev.* 2013,**42**, 3913.
50 H. Djojoputro , X. F. Zhou , S. Z. Qiao , L. Z. Wang , C. Z. Yu , G. Q. Lu , *J. Am. Chem. Soc.* 2006 , **128** , 6320 .
51 L. Zhang, S. Z. Qiao, Y. G. Jin, Z. G. Chen, H. C. Gu, G. Q. Lu, *Adv. Mater.* 2008, **20**, 805.
52 S. Z. Qiao, C. X. Lin, Y. G. Jin, Z. Li, Z. M. Yan, Z. P. Hao, Y. N. Huang, G. Q. Lu, *J. Phys. Chem. C* 2009, **113**, 8673.
53 J. Liu, H. Q. Yang, F. Kleitz, Z. G. Chen, T. Y. Yang, E. Strounina, G. Q. Lu, S. Z. Qiao, *Adv. Funct. Mater.* 2012, **22**, 591.
54 S. Haffer , M. Tiemann , M. Froba , Chem. Eur. J. 2010 , **16** , 10447.
55 W. Guo , J. Wang , S. J. Lee , F. Dong , S. S. Park , C. S. Ha , *Chem. Eur. J.* 2010 ,**16** , 8641 .
56 Y. Yang , J. Liu , X. B. Li , X. Liu , Q. H. Yang , *Chem. Mater.* 2011 , **23** , 3676 .
57 J. Y. Shi, C. A. Wang, Z. J. Li, Q. Wang, Y. Zhang, W. Wang, *Chem. Eur. J.* 2011, **17**, 6206 .
58 Y. Chen, P. F. Xu, H. R. Chen, Y. S. Li, W. B. Bu, Z. Shu, Y. P. Li, J. M. Zhang, L. X. Zhang , L. M. Pan, X. Z. Cui, Z. L. Hua, J. Wang, L. L. Zhang, J. L. Shi, *Adv. Mater.* 2013, **25**, 3100.
59 J. Liu, Q. H. Yang, L. Zhang, H. Q. Yang, J. S. Gao, C. Li, *Chem. Mater.* 2008, **20**, 4268.
60 P. Podsiadlo, S. G. Kwon, B. Koo, B. Lee, V. B. Prakapenka, P. Dera, K. K. Zhuravlev, G. Krylova, E. V. Shevchenko, *J. Am. Chem. Soc.* 2013, **135**, 2435.
61 S. Fujita, S. Inagaki, *Chem. Mater.* 2008, **20**, 891.
62 B. Tan, S. E. Rankin, *J. Phys. Chem. B* 2004, **108**, 20122.
63 Colver, P. J., Colard, C.A. L., Bon, S. A. F. , *J. Am. Chem. Soc.* 2008, 130, 16850.

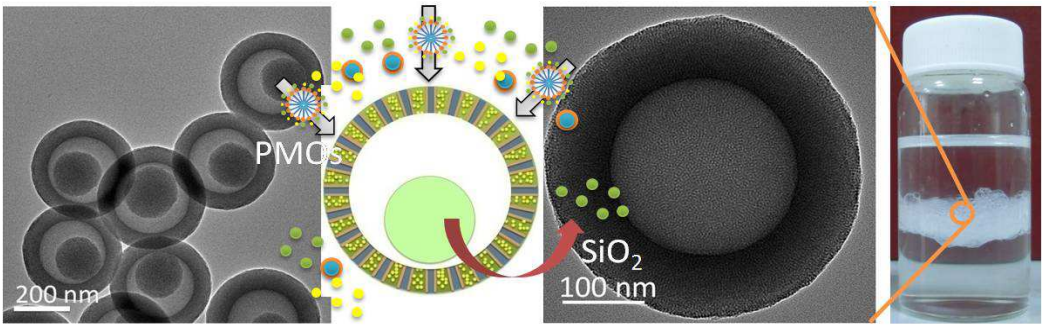

An amphiphilic periodic mesoporous organosilicas hollow shell with perpendicular mesochannels is constructed for application in sorption and catalysis through a novel organosilane-directed growth-induced etching strategy.